



Activation and deformation of immobilized lipase on self-assembled monolayers with tailored wettability

Journal:	<i>Physical Chemistry Chemical Physics</i>
Manuscript ID:	CP-ART-02-2015-000802.R2
Article Type:	Paper
Date Submitted by the Author:	09-Apr-2015
Complete List of Authors:	Chen, Peng-Cheng; Zhejiang University, Department of Polymer Science and Engineering Huang, Xiao-Jun; Zhejiang University, Department of Polymer Science and Engineering Xu, Zhi-Kang; Zhejiang University, Department of Polymer Science and Engineering

SCHOLARONE™
Manuscripts

Activation and deformation of immobilized lipase on self-assembled monolayers with tailored wettability

Peng-Cheng Chen, Xiao-Jun Huang^{*}, Zhi-Kang Xu

MOE Key Laboratory of Macromolecular Synthesis and Functionalization,
Department of Polymer Science and Engineering, Zhejiang University, Hangzhou
310027, China

^{*} Corresponding author. Address: Key Laboratory of Macromolecular Synthesis and Functionalization, Department of Polymer Science and Engineering, Zhejiang University, 38 Zhe Da Road, Hangzhou, 310027, China.
Tel.: +86 571 87952605; fax: +86 571 87951773.
E-mail address: hxjzxh@zju.edu.cn.

Abstract

In this work, lipase from *Candida rugosa* (CRL) was immobilized on self-assembled monolayers (SAMs) with wettabilities varied from high hydrophilicity to high hydrophobicity by adsorption in order to clearly elucidate the interfacial activation character of lipases. The SAMs were made of 11-hydroxyundecane-1-thiol and 1-dodecanethiol. The adsorption behavior was monitored *in situ* by quartz crystal microbalance with dissipation (QCM-D) and enzyme binding constants showed a higher affinity between CRL and more hydrophobic surfaces. Atomic force microscopy (AFM) and X-ray photoelectron spectroscopy (XPS) were used to characterize the morphologies of adsorbed lipases. Amide I band attenuated total reflection/Fourier transformed infrared (ATR/FTIR) spectroscopy showed an increasing fraction of intermolecular β -sheet content on surface with higher hydrophilicity. Moreover, liquid chromatography (LC) verified the activity of CRL adsorbed on hydrophobic surface was higher than that on hydrophilic surface. This work related the enzyme activity to the substrate property, adsorption behavior, distribution, and morphology of lipases, thus helping to achieve an external control of both the immobilization process and enzyme utilization.

1. Introduction

Lipases (EC 3.1.3.3, according to the nomenclature of International Union of Pure and Applied Chemistry) are important enzymes that can catalyze different alcoholysis, hydrolysis, trans-esterifications, aminolysis and enantiomer resolution reactions under

benign experimental and environmental conditions, therefore having been widely applied in the food, pharmaceutical, and detergent industries.¹⁻⁵ Lipases possess chemoselectivity, regioselectivity and stereoselectivity; and compared with traditional chemical catalysts, they are green and thus can meet the requirements of sustainable development of environment and economy. In the last decade, there were more than 2000 publications appearing per year (data obtained from Web of Science (SCI-E/SSCI/A&HCI)). One unique characteristic of lipases is interfacial activation, namely they have only marginal activity toward molecularly dissolved substrates but display high activity when come across an insoluble substrate or a hydrophobic support, (i.e. in the presence of an interface of two distinct phases).⁶⁻⁸ The activity enhancement of lipases by interfaces has greatly fascinated enzymologists and several mechanisms were proposed to explain it, including a proposal stating a conformational change of lipase shifting from a “closed” form to an “open” one at the interface.⁹⁻¹³ Based on this exclusive character of interfacial activation, for a long time and still up to now, various types of hydrophobic supports have been exploited to immobilize lipases for high activity and recoverable biocatalyst simultaneously.¹⁴⁻¹⁶ However, in contrast to the broad spectrum of lipase immobilization using hydrophobic supports, only a few studies have provided general conclusions in terms of structural rearrangements, immobilization kinetics and protein aggregation.¹⁷⁻¹⁸ Therefore, a theoretical understanding of how a lipase interacts with a support is a necessary prerequisite to develop rational design strategies in order to achieve an external control of both the immobilization process and enzyme utilization, and the

interfacial activation of lipases cannot be fully understood unless their action on dissolved substrates is more precisely known.

In this work, we have attempted to draw a comprehensive picture on how lipase immobilization and their activation process are affected by surface wettability. Self-assembled monolayers (SAMs) of methyl-terminated and hydroxyl-terminated alkanethiols were formed on gold chips for the adsorption of lipase from *Candida rugosa* (CRL). The immobilization process and the immobilized lipases were evaluated using complementary techniques – in solution by quartz crystal microbalance with dissipation (QCM-D), in air by atomic force microscopy (AFM) and in vacuum by X-ray photoelectron spectroscopy (XPS). Attenuated total reflection/Fourier transformed infrared (ATR/FTIR) spectroscopy was applied to calculate the secondary structure contents of the immobilized CRL. Moreover, the immobilization and the catalysis kinetics are clearly presented based on analytical technologies of liquid chromatography (LC) and theoretical modeling.

2. Experimental

2.1 Materials

Lipase (from *Candida rugosa*) powder (1150 units/mg solid) and 11-Hydroxyundecane-1-thiol (HUT) were obtained from Sigma-Aldrich Chemical Co. (St. Louis, MO, USA) and used as received. 1-dodecanethiol (DDT) was purchased from Sinopharm Chemical Reagent Co. Ltd. (Shanghai, China) and used without further purification. A 50.0 mM phosphate buffer solution with a pH value of 7.0

(PBS 7.0) was prepared by dissolving 123.7 mg potassium phosphate and 193.7 mg sodium phosphate dibasic in 100 mL water. The water used was purified by filtration through an ELGA Lab Water system (France) and showed a resistivity of 18.2 M Ω -cm. Lipase solution was prepared by dissolving lipase powder in PBS 7.0. All other chemicals were of analytical grade and used without further purification.

QCM-D gold sensor chips were commercially available from Q-SENSE (Sweden). The chips were first cleaned by Piranha solution (98% H₂SO₄/30% H₂O₂ = 7/3, v/v) at ambient temperature for 5-10 min to remove all dust particles and organic contaminants and then thoroughly rinsed with ultra-pure water. Finally, the chips were dried under a steady stream of ultra-pure N₂ gas before use.

2.2 Preparation of self-assembled monolayers (SAMs) on QCM-D chips

SAMs with varied wettabilities were fabricated on the surfaces of clean QCM gold sensor chips. Series of mixed-thiols solutions were blended with different solution ratio of HUT / tetrahydrofuran (THF, 1 mM) and DDT / THF (1 mM). QCM gold sensor chips were immersed into them for ~ 20 h at room temperature for SAMs formation. After that, the chips with different surface composition should be rinsed for three times with THF solution followed by water to remove any unbound thiol molecules. Finally, the chips were dried under N₂.

2.3 Water contact angle (WCA) measurement

The hydrophilicities of different QCM-D chip surfaces were characterized by WCA measurement. WCA was determined using a CTS-200 system (Cellcons Controls,

China) fitted with a drop shape analyzer at room temperature by sessile drop method, as follows. A water droplet (2.0 μL) was placed on a chip surface from a needle tip, and images of the droplet were shot. WCAs were calculated from these images with software. Each reported value was the average of at least five independent measurements.

2.4 X-ray photoelectron spectroscopy (XPS) measurement

XPS was used to detect elemental composition of the SAM. This experiment was carried out on a RBD upgraded PHI-5000C ESCA system (Perkin Elmer) with Al $K\alpha$ radiation ($h\nu = 1486.6$ eV). The base pressure of the analyzer chamber was about 5×10^{-8} Pa. Both the whole spectra and the narrow spectra of all the elements were recorded by using RBD 147 interface (RBD Enterprises, USA) through the AugerScan 3.21 software. Binding energies were calibrated by using the bulk Au $4f_{7/2}$ peak at 84.00 eV.

In order to character the CRL immobilized on SAMs, XPS measurements were performed on an Axis Ultra spectrometer (Kratos Analytical, UK) employing a hemispherical analyzer for spectroscopy and a spherical mirror analyzer for imaging. Images were acquired with a monochromated Al $K\alpha$ source at pass energies of 160 eV for survey spectra and 80 eV for core level spectra. The binding energy was corrected for static charging of C1s peak at 284.6 eV. The XPS images were acquired for $200 \mu\text{m} \times 200 \mu\text{m}$ area at a pass energy of 80 eV. The background-corrected image was obtained by subtraction of the background region image from the image at

the peak of interest. The data processing was done using Casa XPS (Casa Software LTD.).

2.5 CRL adsorption behavior on SAMs by quartz crystal microbalance with dissipation (QCM-D)

CRL immobilization experiments were conducted in real time and in situ using a Q-SENSE E1 system (Q-SENSE, Sweden). The quartz crystal (AT-cut) with a fundamental resonance frequency of 5 MHz and a diameter of ~14 mm was mounted in a fluid cell with one side exposed to the solution. A peristaltic pump was used to deliver liquids to the channel of the flow cell. First, a stable baseline signal was established by flowing a 50.0 mM phosphate buffer solution at pH 7.0 (PBS 7.0) at a rate of 25 $\mu\text{L}/\text{min}$ through the sensor. Then, lipase solution was injected into the channel at the same flow rate. After immobilization process, PBS 7.0 was used to remove loosely bound enzymes from the chip surface.

The resonator had a mass sensitivity constant (C) of $17.7 \text{ ng cm}^{-2} \text{ Hz}^{-1}$. The addition of a small layer to the electrodes would induce a decrease in resonance frequency (Δf) which is proportional to the mass change (Δm) of the layer. In vacuum or air, for a rigidly adsorbed layer which is evenly distributed and much thinner than the crystal, Δf is related to Δm and the overtone number ($n = 1, 3, 5, \dots$) by the Sauerbrey equation of $\Delta m = -C \frac{\Delta f}{n}$. The change in dissipation factor (ΔD) is determined based on the fact that the voltage over the crystal decays exponentially as a damped sinusoidal when the driving power of a piezoelectric oscillator is switched

off.

In this study, the values reported throughout for Δf and ΔD were measured at the third overtone, with the working temperature maintained at 25 °C. Raw data were analyzed with Origin 7.0 (Origin-Lab, USA) and Q-Tools software (Q-SENSE).

2.6 Atomic force microscopy (AFM) measurements

AFM (Nano IV, Veeco, USA) was used to study the surface morphology of different CRL-immobilized QCM-D chip surfaces. The AFM observation was performed under nitrogen protection at room temperature using a TM Lumina atomic force microscope operated in tapping mode. Oxide sharpened SiN₃ cantilevers were used with a quoted spring constant of 0.04 N m⁻¹. Data were captured at a rate of 10 m s⁻¹ in the z direction and a scan rate of 4 Hz. All images are shown in the height mode.

2.7 Attenuated total reflection/Fourier transformed infrared (ART/FTIR) spectral analysis of the immobilized CRL

ART/FTIR spectroscopy was used to quantify the secondary structure content of CRL adsorbed on SAMs with varied wettabilities. The spectra were collected in the 1000–4000 cm⁻¹ range with a Nicolet Nexus470 (Madison, WI). After each experiment, the exposed surface of the germanium surface with cleaned successively with deionized water, 1% (w/w) sodium dodecyl sulfate solution, deionized water, 50% (w/w) aqueous ethanol solution and finally dried with air.¹⁹

2.8 Evaluating the CRL activity by liquid chromatography (LC)

After CRL immobilization on SAM-modified QCM-D chips, enzyme-catalyzed

hydrolysis reactions were studied using triacetine (TA) as the model substrate. TA solution was injected into the channel at a flow rate of 25 $\mu\text{L}/\text{min}$ at 25 $^{\circ}\text{C}$. After hydrolysis reaction, ultra pure water was used to remove both the hydrolysis product and the un-reacted TA from the chip surface. Moreover, a blank control was conducted on SAM-modified QCM-D chips without CRL immobilization.

The hydrolysis reaction was run for 20 min, and the effluent liquid was collected and analyzed on a ZORBAX SB_C₁₈ (3.5 μm , 2.1 \times 100 mm) column (the injection volume was 20 μL for each sample). A $V(\text{ultra pure water}) : V(\text{acetonitrile}) = 70 : 30$ mixed solvent was used as the mobile phase at a flow rate of 0.15 mL/min. The mobile phase was delivered by the Agilent 1100 LC system at 25 $^{\circ}\text{C}$ and monitored at 210 nm using a diode-array detector. The data was acquired by HP ChemStation software system using an HP KAYAK XA PC computer.

One CRL unit corresponded to the hydrolysis of 1 μmol TA per minute under the assay conditions. Standard concentration of TA was used to construct a calibration curve. The specific activity for CRL was defined as the number of CRL units per milligram of protein. Activity retention value was the ratio of specific activity of immobilized CRL to that of free one. Each data was the average of at least three parallel experiments, and the standard deviation was within ca. $\pm 5\%$.

3. Results and discussion

3.1 Surface wettability of SAMs

The self-assembly method presents exciting possibilities for engineering surfaces with

controllable physicochemical properties. According to Figure 1, a gradual variation of surface wettability from hydrophilic to hydrophobic character was shown by modifying the gold surface using the mixtures of methyl- and hydroxyl-terminated alkanethiols with different relative concentrations in THF.^{20–23} The WCA of bare Au surface was $47.3 \pm 0.8^\circ$. The homo HUT SAM showed a WCA of lower than 20.0° ; incorporated DDT brought about an increase in WCAs and the sample with the highest WCA of $105.9 \pm 2.7^\circ$ referred to the homo DDT SAM. These differences in wettability reflected the success of mixed-thiols SAM processes to the formation of mixed functional groups modified model surfaces. Subsequently, XPS was applied to accurately detect the surface composition. Figure S1 was the narrow spectra of elements O_{1s} and C_{1s} with high resolution for the five differently composited SAMs. The O_{1s} peak decreased with the increasing molar fraction of DDT (χ_{DDT}) in THF solution, indicating the χ_{DDT} of the mixed monolayer on the surface increased with the increment of χ_{DDT} in the solution. For a smooth surface consisting of two components, its WCA can be calculated according to Cassie equation ($\cos \theta_C = f_1 \cos \theta_1 + f_2 \cos \theta_2$, where f_i is the fraction area of the surface with a contact angle of θ_i). The calculated WCAs, as shown in Figure S2, were very close to those measured ones, meaning the ratio of methyl-terminated group on the surface is nearly same as the DDT ratio in the mixed-thiols solution. All these results verified that the hydrophobic or hydrophilic constituent density can be easily controlled by adjusting the corresponding methyl- or hydroxyl-terminated alkanethiol ratio in the solution.

-- Figure 1 --

3.2 CRL adsorption behavior

It has been known that protein adsorption usually involves multipoint electrostatic, hydrophobic, and hydrogen-bonding interactions between protein molecules and surface. In this work, all the protein adsorption were performed under pH 7.0, thus the hydroxyl group at the end of HUT will maintain an uncharged state during the protein adsorption because its pK_a is about 13. Moreover, at this pH, CRL becomes negatively charged due to the deprotonation of carboxylic acid groups, which would weaken hydrogen-bonding interaction between the protein and the surface. Based on these facts, the electrostatic and hydrogen-bonding interactions would be largely screened, and the self-assembling surfaces should be applicable to the study of surface wettability effect on CRL adsorption in this work. QCM-D was used as a label-free read-out method to evaluate the adsorption process of CRL (ESI, Figure S3). ΔD is related to the structure of protein layer on the surface: a rigid and dense protein layer gives rise to a small dissipation factor, whereas a soft and swollen protein layer leads to a larger one. Besides, for the protein molecules with a similar structure on the surface, the larger the amount of adsorbed protein is, the higher the value of ΔD can be. For each sample in this work, Δf on all overtones ($n = 3, 5, 7, 9$) were similar with small dissipation values less than 6×10^{-6} , so the adsorbed protein mass can be calculated according to the Sauerbrey equation. Δf reflected the absorbed lipase mass and were dependent on the enzyme concentration (ESI, Figure S4). The enzyme binding (k_{on}) and dissociation (k_{off}) constants can be calculated Equation S1-S3, and the results are shown in Figure 2. For each SAM on which CRL adsorbed, k_{on} value

was bigger than k_{off} . Moreover, the ratio of k_{on} to k_{off} reflected the binding constant of CRL, and this value increased with an increase in SAM hydrophobicity, indicating CRL is more prone to adsorb on a hydrophobic surface.

-- Figure 2 --

Two models were employed to analyze the CRL adsorption dynamics, viz. the pseudo-first order model in which a protein reversibly interacts with the surface and binding sites possess homogenous affinities, and the biphasic model which considers both a stable, tight protein–surface complex and a loose one (ESI, Figure S5, Equation S4-S11).^{24–26} The adsorption profile obtained from QCM-D measurements can be fitted to these two theoretical models. Since it is difficult to detect experimentally the presence of tightly and loosely bound surface populations in a biphasic model, a nonlinear regression analysis was undertaken. The protein concentration was maintained at 0.05 mg/mL during the adsorption process, at this concentration, the loadings of CRL adsorbed on the SAMs were less than the maximum loading when CRL array in monolayer. Table 1 summarizes the fitting parameters. When the support was solely composed of HUT, the CRL adsorption profile was in closer agreement with the biphasic model (Figure 3(a)), and displayed a much lower forward rate constant value for tightly bound proteins (k_1 , $8.80 \times 10^{-3} \text{ s}^{-1}$) than that for loosely bound protein (k_2 , 0.181 s^{-1}), revealing the dominance of loosely bound CRL on this support. In this case, the heterogeneity of the binding points on the CRL molecule surface to the support causes the deviation from the pseudo-first order model. Increasing the hydrophobicity of the support caused the k_1 value to increase,

thereby suggesting a stronger interaction between the CRL and the support and also an increasing amount of tightly bound CRL. On a homo DDT support, the CRL adsorption profile fitted well with both the pseudo-first order model and the biphasic model (Figure 3(e)). Moreover, the data analysis for k_2 yielded a negative value which finally reached 0, indicating almost no loosely bound CRL.

We theorize that the primary driving force for CRL adsorption on this support came from the hydrophobic interactions between the hydrophobic domain of CRL (the catalytic site) and the support, which formed the tight protein–surface complexes.

-- Figure 3 --

-- Table 1 --

Two distinct kinetic processes usually operate during protein adsorption – the fast binding of the protein molecules onto the support and the subsequent structural rearrangements or conformational changes within the adsorbed layer.^{27–29} In the $\Delta D - \Delta f$ plot, they were reflected by two different slopes of k_4 and k_5 , respectively (ESI, Figure S6). The values of k_4 and k_5 are recorded in Figure 4. The value of k_5 was an indicator of the deformation degree of the immobilized CRL. It decreased with an increase in χ_{DDT} on the surface, indicating an interesting phenomenon that a more hydrophobic surface helped to maintain the structure of adsorbed CRL. It was also noted that when the support was composed of 100% DDT, the CRL formed a monolayer and almost no protein deformation was observed.

-- Figure 4 --

3.3 Morphology and distribution of immobilized CRL

AFM was used as a complement to the dynamic information of QCM-D to obtain protein distribution and morphology information. In AFM measurements, the morphology of the adsorbed protein can be viewed, and the protein layer height can be got by cross-sectional survey, as was presented in Figure S7. The SAM surfaces were incompletely covered by CRL clusters, and the surface domain with no adsorption was the pristine SAM because its roughness value was similar to that of the pristine SAM. The dimensions of a CRL molecule are $6.5 \text{ nm} \times 9.8 \text{ nm} \times 17.6 \text{ nm}$ from the crystal structure data.³⁰ On a homo DDT surface, the adsorbed CRL form in clusters of several CRL molecules and the maximum step height between the clusters and SAM was 8.33 nm (Figure 5). This value was close to the two shorter axes of CRL, suggesting that the protein cluster did not grow vertical to the substrate but rather grew along the in-plane direction. The above results can be explained considering the CRL structural changes as follows. In solution, generally the outer surface of CRL is hydrophilic to make it dissolve well and the relatively hydrophobic catalytic site is usually buried inside.³¹ In the present work, the hydrophobic surface induces the exposure of the hydrophobic domain of CRL to interact with the support, which plays an important role as the driving force for CRL adsorption and thus resulting the regular array of adsorbed CRL. Moreover, the affinity between the hydrophobic domain of CRL and the hydrophobic surface is larger than the aggregation forces among the CRL molecules. The decrease in the surface hydrophobicity led to the formation of larger size of CRL clusters and an increase in

the step heights, indicating a vertical growth of the adsorbed CRL on the surfaces. In such cases, the hydrophobic interaction between the surface and CRL was abated and the van der Waals force of the CRL clusters made the CRL aggregation and piling possible. Significantly, the AFM results in this work verified the conformational changes of CRL suggested by immobilization kinetics.

-- Figure 5 --

XPS imaging was further applied to observe the adsorbed CRL, and the results were shown in Figure 7. The scale bar is 50 μm so that we cannot get the distribution of proteins as clearly as AFM, but it gives some information in a larger dimension. From this figure we can know that more CRL were adsorbed on surfaces with higher hydrophobicity. And for the relatively hydrophilic surfaces bearing 0% ~ 50% DDT, we can clearly see the difference between CRL and the surface, and the brightness of the N_{1s} signal varied much on one surface, meaning there existed uneven protein aggregations; while for the hydrophobic surfaces bearing 75% and 100% DDT, the adsorbed CRL and the N_{1s} signal array relatively regularly.

-- Figure 6 --

In order to verify the protein aggregation and corresponding structural perturbation on surface, ATR/FTIR spectroscopy was used to quantify the secondary structure content of CRL adsorbed on the five different SAMs. It is known that the protein structure reference spectra are generated in the amide I (1600–1700 cm^{-1}) and amide III (1200–1300 cm^{-1}) bands. Amide I band estimates are usually better than

amide III band estimates, hence, amide I band is used here. A second derivative analysis to locate peaks due to secondary structural components was adopted.³² Figure S8 presented the raw spectra for the amide I region, and second derivative of the spectra was shown in Figure 7(a). The mean peak positions were α -helix (1656 cm^{-1}), intramolecular β -sheet (1693 and 1633 cm^{-1}), unordered and ordered helix (1672 , 1648 and 1620 cm^{-1}) and turn structures (1720 , 1668 , 1630 and 1617 cm^{-1}).³³ Notably, the peaks at 1627 cm^{-1} and 1622 cm^{-1} indicated the formation of intermolecular contacts. According to Figure 7(a), the peak for α -helix (which belonged to the native CRL) decreased, meanwhile that for intermolecular β -sheet increased when the surface got more hydrophilic. The calculated intermolecular β -sheet fraction on different surfaces, obtained from the area under the second derivative peak ($\sim 1627\text{--}1622\text{ cm}^{-1}$) was shown in Figure 7(b). As expected, the extent of protein aggregation increased with increasing hydrophilicity, also the ATR/FTIR analysis indicated that surfaces that strongly perturbed the native protein structure also aid in aggregation.

-- Figure 7 --

For the first time, to the best of our knowledge, the current research provided a direct and detailed evaluation of the lipase activation and deformation character through enzyme immobilization kinetics and structural analysis.

3.4 Activity of immobilized CRL

Subsequently, TA was used as the substrate for analyzing the catalytic kinetics of the immobilized CRL. Aqueous solutions of TA with concentrations less than 0.3 M were

prepared so that the TA dissolves completely to form a homogeneous solution and hydrolysis reaction was studied by both QCM-D and liquid chromatography (LC) (ESI, Figure S9). According to Figure 8(a), the typical peak for TA was at 13.7 min. After the CRL-catalytic reaction, the peak area for TA decreased and three new peaks appeared at 3.5 min, 4.3 min and 5.6 min, which were ascribed to the hydrolytic products of TA. CRL activity was obtained based from the rate of hydrolysis of TA (ESI, Figure S10). The liquid chromatograms of TA before and after hydrolysis reaction showed that more TA was hydrolyzed when CRL was immobilized on hydrophobic surfaces (ESI, Figure S11). To be more precise, the catalytic kinetics can be expressed by the Michealis–Menten model and the Michaelis constant (K_m) and the maximum hydrolysis reaction rate (V_{max}) were calculated (ESI, Equation S12),^{34–35} and the results are presented in Figure 9. K_m values for the immobilized CRL were higher than that for the free one, which was reasonable since the support increased the mass transfer resistance of the substrate and products.³⁶ Importantly, the values for V_{max} increased significantly with the increment of SAM hydrophobicity. For example, when CRL was immobilized on 100% DDT support, the V_{max} value was 45.14 U/mg, which was 6.5 times higher than that for the 0% DDT support. Moreover, the specific activities (shown in Figure S12) and activity retention of the immobilized CRL can be calculated based on the hydrolysis reaction rates. According to Figure 8(b), the activity of CRL immobilized on 0% DDT surface was only 9.8% compared with the free CRL; whereas, when the DDT percentage was 50%, it increased 5.6 times, and on 100% DDT support, the value was as high as 116.3%. The catalytic

efficiency concurred with the aforementioned kinetics and morphology measurements and verified the activation of CRL immobilized on a hydrophobic support.

-- Figure 8 and 9 --

One pioneering work done by Reis et al. used three different SAM surfaces for lipase-catalyzed reactions.³⁷ Surface plasmon resonance was used for the first time to monitor the enzyme immobilization as well as catalyzing process *in situ*. They showed that the hydrophobic surface bound more lipases. Moreover, both the surface wettability and the mode of enzyme attachment strongly influence the product composition. While in our work, the emphasis was put on the aggregation and structural deformation when lipase were immobilized onto surface, showing that CRL is more prone to adsorb on a hydrophobic support. And the CRL adsorbed on the 100% DDT surface underwent least structural deformation, and the hydrophobic surface can induce the activation of CRL.

4. Conclusions

This work systematically studied the effect of surface wettabilities on CRL immobilization behavior and exhibited the morphology of immobilized CRL in detail. By tailoring the relative concentrations of methyl- and hydroxyl-terminated alkanethiols in solution, SAMs with contacting angles gradually varied from 20° to 105.9° was constructed and used for CRL adsorption. CRL is prone to adsorb on a hydrophobic support with a higher enzyme binding constant / dissociation constant ratio, and the hydrophobic interaction can induce the exposure of hydrophobic

catalytic site and lay the protein evenly and regularly, which activate the CRL; while lipases exist in aggregation and undergo deformation on a hydrophilic support, which is unfavorable for their activity. On the most hydrophobic surface constructed by pure DDT, the activity retention of the immobilized CRL was 116.3%, which was higher than that of the free CRL and was 10.9 time higher than that of the CRL immobilized on the 0% DDT surface.

Acknowledgements

Financial support is acknowledged to the National Natural Science Foundation of China (Grant no. 51473143).

Notes and references

- 1 D, Goswami, J. K. Basu and S. De, *Crit. Rev. Biotechnol.*, 2013, **33**, 81.
- 2 P. Reis, K. Holmberg, H. Watzke, M. E. Leser and R. Miller, *Adv. Colloid Interfac.*, 2009, **147–148**, 237.
- 3 K. P. Dhake, A. H. Karoyo, M. H. Mohamed, L.D. Wilson and B. M. Bhanage, *J. Mol. Catal. B: Enzym.*, 2013, **87**, 105.
- 4 P. C. Chen, X. J. Huang and Z. K. Xu, *RSC Adv.*, 2014, **4**, 6151.
- 5 P. Reis, K. Holmberg, R. Miller, J. Kragel, D. O. Grigoriev, M. E. Leser and H. Watzke, *Langmuir*, 2008, **24**, 7400.
- 6 L. Sarda and P. Desnuelle, *Biochim. Biophys. Acta*, 1958, **30**, 513.
- 7 B. Entressangles and P. Desnuelle, *Biochim. Biophys. Acta*, 1974, **341**, 437.
- 8 L. Chronopoulou, G. Kamel, C. Sparago, F. Bordi, S. Lupi, M. Diociaiuti and C.

-
- Palocci, *Soft Matter*, 2011, **7**, 2653.
- 9 A. M. Brzozowski, U. Derewenda, Z. S. Derewenda, G. G. Dodson, D. M. Lawson, J. P. Turkenburg, F. Bjorkling, B. Huge-Jenson, S. A. Patkar and L. Thim, *Nature*, 1991, **351**, 492.
- 10 P. Reis, R. Miller, J. Kragel, M. E. Leser, H. Watzke, V. B. Vainerman and K. Holmberg, *Langmuir*, 2008, **24**, 6812.
- 11 A. G. Cunha, M. D. Besteti, E. A. Manoel, A. A. T. da Silva, R. V. Almeida, A. B. C. Simas, R. Fernandez-Lafuente, J. C. Pinto and D. M. G. Freire, *J. Mol. Catal. B: Enzym.*, 2013, **100**, 59.
- 12 K. Hernandez, C. Garcia-Galan and R. Fernandez-Lafuente, *Enzyme Microb. Tech.*, 2011, **49**, 72.
- 13 P. Reis, R. Miller, M. E. Leser, H. Watzke, V. B. Vainerman and K. Holmberg, *Langmuir*, 2008, **24**, 5781.
- 14 R. Jia, Y. Hu, L. Liu, L. Jiang, B. Zou and H. Huang, *ACS Catal.*, 2013, **3**, 1976.
- 15 J. Q. Wang, G. Meng, K. Tao, M. Feng, X. B. Zhao, Z. Li, H. Xu, D. H. Xia and J. R. Lu, *Plos One*, 2012, **7**, e43478.
- 16 W. Feng, X. C. Sun and P. J. Ji, *Soft Matter*, 2012, **8**, 7143.
- 17 R.C. Rodrigues, C. Ortiz, A. Berenguer-Murcia, R. Torres and R. Fernandez-Lafuente, *Chem. Soc. Rev.*, 2013, **42**, 6290.
- 18 V. Ferrario, C. Ebert, L. Knapic, D. Fattor, A. Basso, P. Spizzo and L. Gardossi, *Adv. Synth. Catal.*, 2011, **353**, 2466.
- 19 G. Vedantham, H. G. Sparks, S. U. Sane, S. Tzannis and T. M. Przybycien, *Anal.*

-
- Biochem.*, 2000, **285**, 33.
- 20 A. Ulman, *Thin Solid Films*, 1996, **273**, 48.
- 21 V. Lebec, J. Landoulsi, S. Boujday, C. Poleunis, C. M. Pradier and A. Delcorte, *J. Phys. Chem. C*, 2013, **117**, 11569.
- 22 X. W. Wang, G. M. Liu and G. Z. Zhang, *Langmuir*, 2012, **28**, 14642.
- 23 X. L. Liu, L. Yuan, D. Li, Z. C. Tang, Y. W. Wang, G. J. Chen, H. Chen and J. L. Brash, *J. Mater. Chem. B*, 2014, **2**, 5718.
- 24 S. G. Thakurta, H. J. Viljoen and A. Subramanian, *Thin Solid Films*, 2012, **520**, 2200.
- 25 I. E. Svendsen, L. Lindh and T. Arnebrant, *Colloids Surf. B Biointerfaces*, 2006, **53**, 157.
- 26 A. Tsargorodskaya, A. V. Nabok and A. K. Ray, *Nanotechnology*, 2004, **15**, 703.
- 27 S. V. Orski, S. Kundu, R. Gross and K. L. Beers, *Biomacromolecules*, 2013, **14**, 377.
- 28 F. Hook, M. Rodahl, P. Brzezinski and B. Kasemo, *Langmuir*, 1998, **14**, 729.
- 29 E. Casero, L. Vazquez, A. M. Parra-Alfambra and E. Lorenzo, *Analyst*, 2010, **135**, 1878.
- 30 P. Grochulski, Y. Li, J. D. Schrag, F. Bouthillier, P. Smith, D. Harrison, B. Rubin, M. Cygler, *J. Biol. Chem.*, 1993, **268**, 12843.
- 31 P. Grochulski, Y. G. Li, J. D. Schrag and M. Cygler, *Protein Sci.*, 1994, **3**, 82.
- 32 M. Stefani and C. M. Dobson, *J. Mol. Med.*, 2003, **81**, 678.
- 33 A. Sethuraman and G. Belfort, *Biophys. J.*, 2005, **88**, 1322.

-
- 34 P. C. Chen, X. J. Huang, F. Huang, Y. Ou, M. R. Chen and Z. K. Xu, *Cellulose*, 2011, **18**, 1563.
- 35 Z. P. Han, J. Fu, P. Ye and X. P. Dong, *Enzyme Microb. Tech.*, 2013, **53**, 79.
- 36 K. C. Badgajar and B. M. Bhanage, *Enzyme Microb. Tech.*, 2014, **57**, 16.
- 37 P. Reis, K. Holmberg, T. Debeche, B. Folmer, L. Fauconnot and H. Watzke, *Langmuir*, 2006, **22**, 8169.

Table 1. Kinetic parameters estimated from non-linear regression fitting.

SAM sample		0% DDT	25% DDT	50% DDT	75% DDT	100% DDT
Pseudo-first order	k_1	8.33×10^{-3}	1.12×10^{-2}	1.47×10^{-2}	3.18×10^{-2}	4.36×10^{-2}
	k_{-1}	2.16×10^{-3}	1.58×10^{-3}	1.56×10^{-3}	9.67×10^{-4}	3.18×10^{-4}
	R^2	0.981	0.985	0.988	0.991	0.997
	SS	32.4	20.8	18.7	16.8	4.33
Biphasic	k_1	8.80×10^{-3}	8.75×10^{-2}	0.257	0.316	0.674
	k_{-1}	6.33×10^{-3}	1.71×10^{-3}	1.68×10^{-3}	2.03×10^{-3}	4.38×10^{-3}
	k_2	0.181	8.73×10^{-2}	7.84×10^{-2}	1.90×10^{-3}	0
	k_{-2}	2.75×10^{-3}	0	1.70×10^{-3}	0	0
	k_3	5.92×10^{-3}	9.47×10^{-3}	2.56×10^{-3}	0	0
	R^2	0.998	0.997	0.999	0.999	0.998
	SS	2.11	4.70	3.03	1.51	1.50

Figure Captions

Figure 1. Relationship between the water contact angle on the surface and the molar fraction of 1-dodecanethiol (χ_{DDT}) in the THF solution. The inserted images were the photographs of the water droplets.

Figure 2. The values of enzyme binding constant (k_{on}) and enzyme dissociation constant (k_{off}) as a function of χ_{DDT} on the surface.

Figure 3. Curve-fit of the adsorption profile obtained from QCM-D measurements to the theoretical models.

Figure 4. Changes of the slopes of the ΔD — $-\Delta f$ plots for the first (k_4) and second (k_5) kinetic processes as a function of χ_{DDT} on the surface (ΔD is change in dissipation factor and Δf is change in resonance frequency).

Figure 5. Step height and maximum step height between the adsorbed CRL and original surface of SAM-modified QCM chips.

Figure 6. N_{1s} elemental images ($200 \mu\text{m} \times 200 \mu\text{m}$) of lipase immobilized on surfaces with increasing χ_{DDT} . (a) χ_{DDT} : 0%; (b) χ_{DDT} : 25%; (c) χ_{DDT} : 50%; (d) χ_{DDT} : 75%; (e) χ_{DDT} : 100%. The scale bar presents $50 \mu\text{m}$.

Figure 7. (a) Superimposed second derivative of ATR/FTIR spectra (all spectra were normalized from 1700 – 1600 cm^{-1}) of CRL immobilized on surfaces with varied χ_{DDT} (1~5: χ_{DDT} from 0% to 100%); (b) fraction of intermolecular β -sheet of immobilized CRL obtained from the second derivative peak area (1627 – 1622 cm^{-1}) versus the

surface wettability (1~5: χ_{DDT} from 0% to 100%).

Figure 8. (a) Typical liquid chromatograms of HAc, TA and TA after lipase-catalytic reaction; (b) activity retention of CRL immobilized on SAMs with different wettabilities, the orange dash line refers to the value for free CRL (TA solution concentration: 0.2 M).

Figure 9. Lineweaver-Burk plots for CRL immobilized on SAMs with different wettabilities.

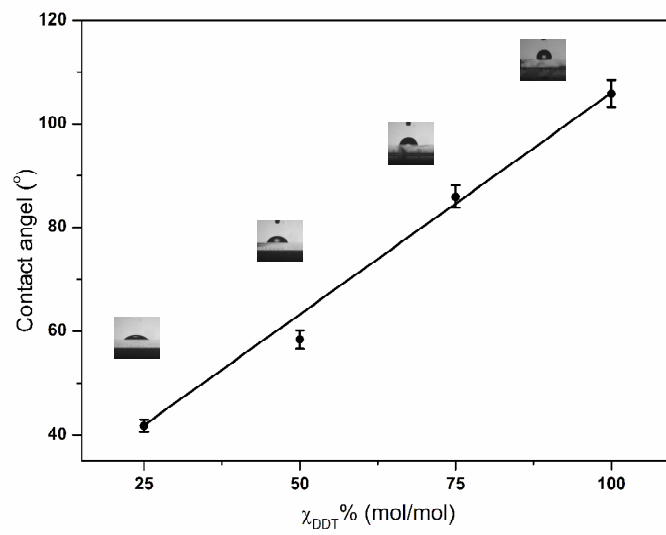


Figure 1

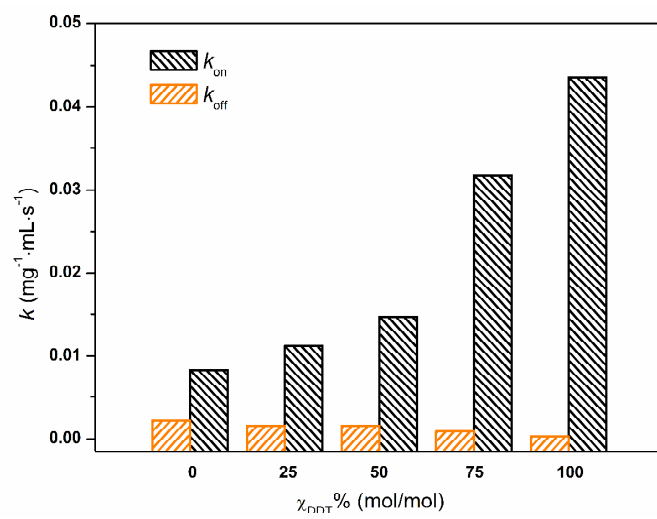


Figure 2

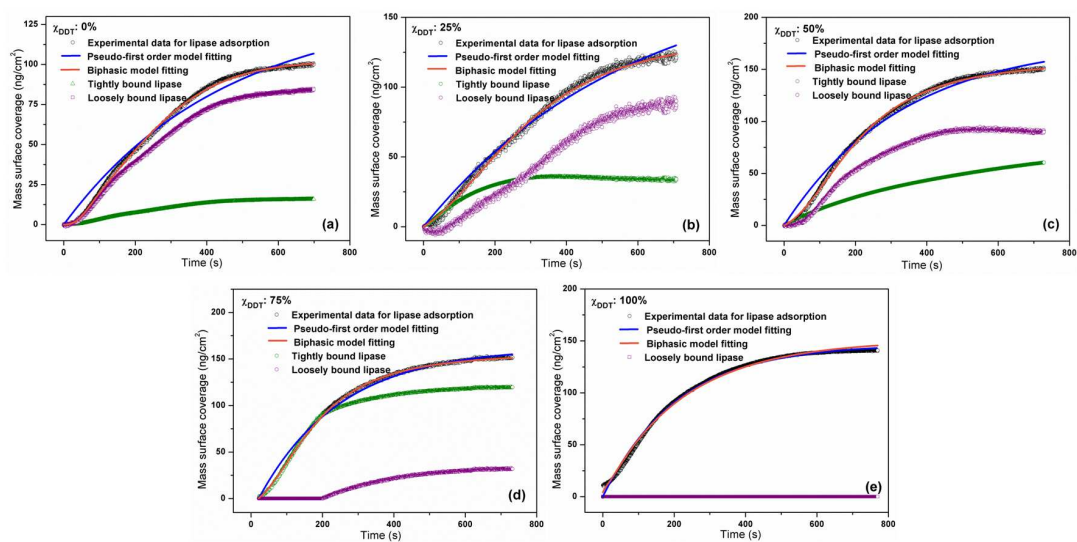


Figure 3

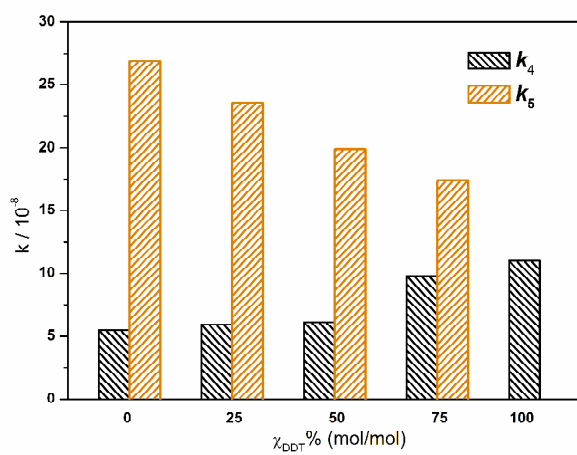


Figure 4

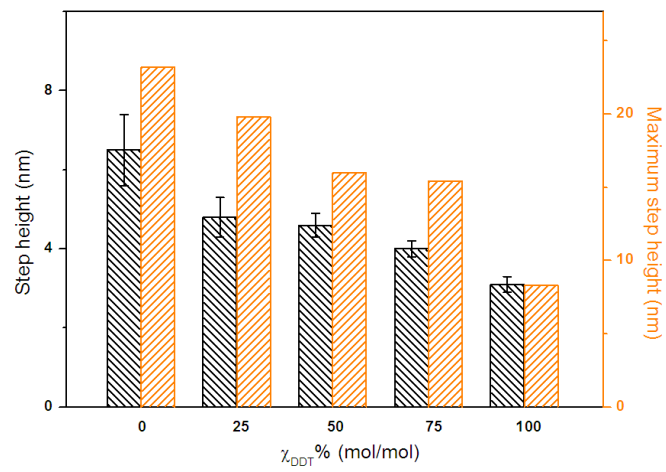


Figure 5

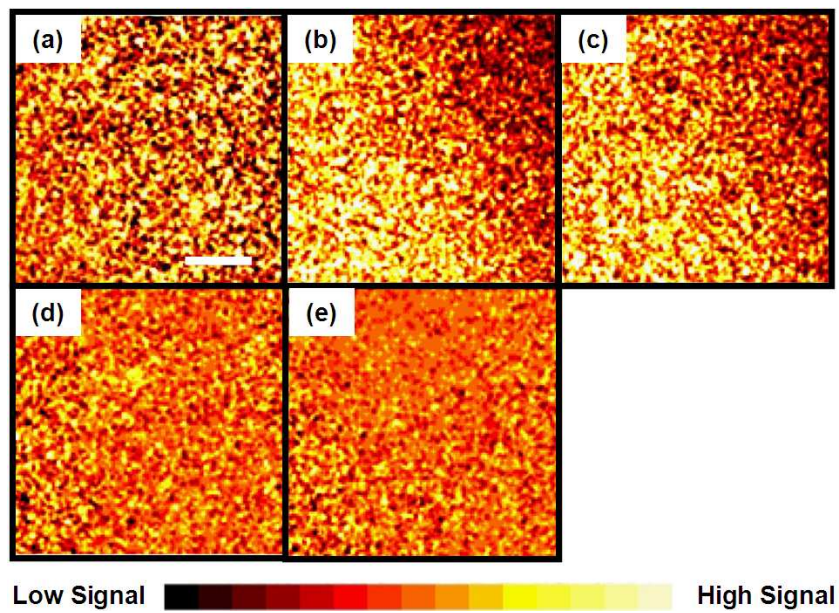


Figure 6

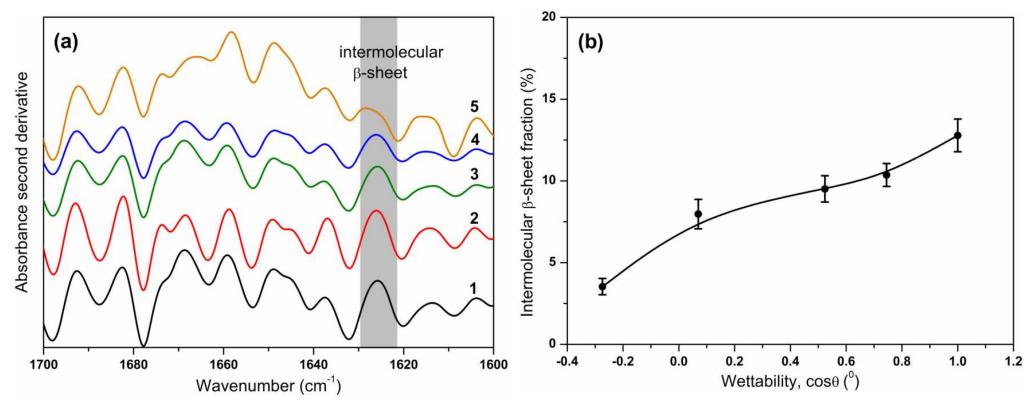


Figure 7

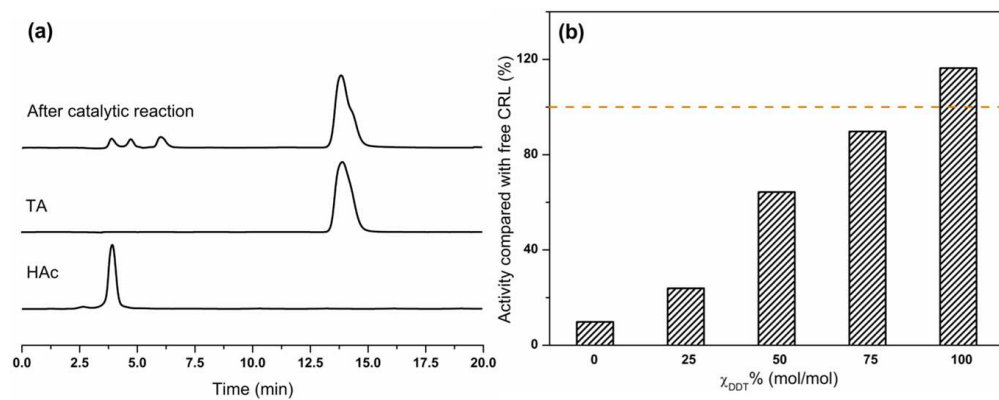


Figure 8

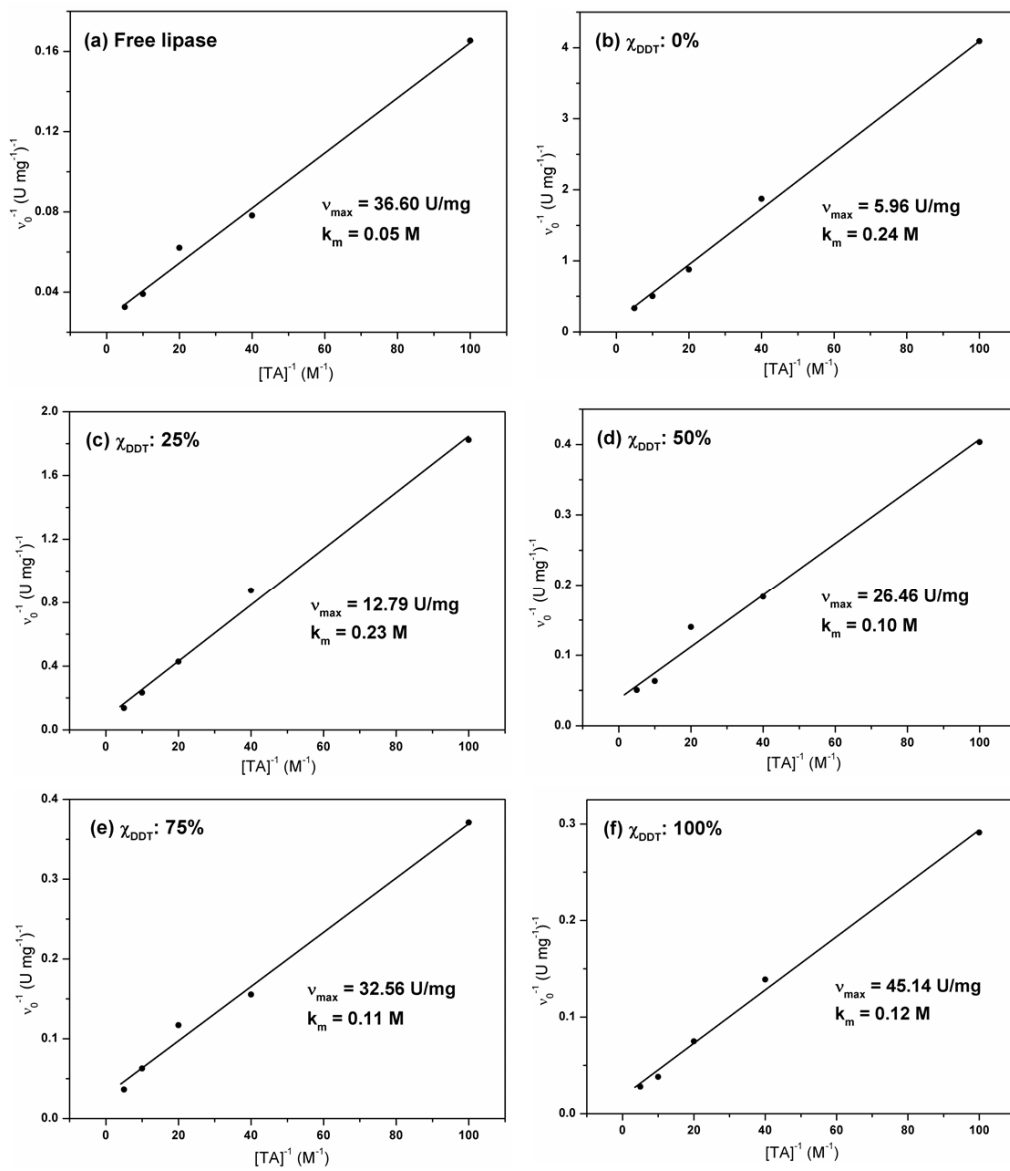


Figure 9